A Composite Mesoscale Cumulonimbus Budget

By

Alan K. Betts

Department of Atmospheric Science
Colorado State University
Fort Collins, Colorado

Colorado State University

Department of Atmospheric Science

Paper No. 186

A COMPOSITE MESOSCALE CUMULONIMBUS BUDGET

by

A. K. Betts

The research for the Venezuelan International Meteorological and Hydrological Experiment (VIMHEX I) was sponsored by the Office of Naval Research under Contract No. N00014-68-A-0493-0002 with Colorado State University. Partial support for the theoretical analysis was received from the Atmospheric Sciences Section, National Science Foundation under Grant No. GA-11637 to Colorado State University.

Atmospheric Science Paper No. 186

Department of Atmospheric Science
Colorado State University
Fort Collins, Colorado

May 1972

TITLE:

A Composite Mesoscale Cumulonimbus Budget

TABLE OF CONTENTS

Table of Contents (cont.) Page

SYMBOL LIST

T	temperature
θ	potential temperature
θ_E	equivalent potential temperature
p	pressure
r	water vapor mixing ratio
ρ	density
Q	a conserved quantity
∇	3-D divergence operator
$\mathbf{v}$	vector wind (3-D)
w	vertical velocity
ω	$-\rho g w$
g	acceleration due to gravity
C_p	specific heat of dry air
L	latent heat of vaporisation of water
z	height co-ordinate
t	time

Model - Fig. 1

A_1	area: region 1 (contains echo)
A_2	area: region 2 (environment)
A_o	echo area
A_R	working area of radar
ℓ_1	circumference of region 1 ($4\pi R$)
ℓ_2	circumference of region 2
$\Delta\ell$	$= \pi R/3$
R	mean echo radius (used to scale $\hat{R}$)
$\hat{R}$	non-dimensional radius from echo center

C	radial velocity on 1, 2 boundary (positive outwards)
τ	mean echo half lifetime
N	mean number of echos/day
Δt	mean length of echo period/day

Other Symbols

$\sim$	large-scale average (including several clouds and their environment)
$\overline{1}$	average over region 1 (model)
$\overline{2}$	average over region 2 (model)
$\overline{}$	large-scale and 17 day average (except in 5.1, 5.2)
$\overline{-1}$	average over region 1 and 17 days data
$\overline{-2}$	average over region 2 and 17 days data
$*$	a value of ω, scaled to $\begin{cases}\text{echo area } A_o \\ \text{echo half-lifetime } \tau\end{cases}$
$'$	a deviation from an area-mean
$\hat{\omega}$	defined in 6.1
$\sum_L$	denotes sum over life-time of echo
$\sum_i$	a sum over pressure increments
$\sum_k$	a sum over 12 values on ℓ_1

ABSTRACT

Composite maps at levels from 950 mb to 150 mb of relative wind field, mixing ratio (r), equivalent potential temperature (θ_E) and temperature perturbation fro the growth and decay phases of a mean mesoscale cumulonimbus system (systems used had a maximum radar echo area >400 km^2) were constructed using radar and one rawinsonde (experiment VIMHEX) for days having a similar synoptic scale wind field. Echo area and track were measured from radar film, relative winds calculated by subtracting a mean echo velocity; positions of radiosonde data points relative to echo as center were computed, scaled by an echo radius, and plotted with echo motion vectors aligned along one coordinate axis. Mass flows into the mean system at all levels give vertical mass transports for growth and decay phases, and net mass balance. The net convergence of r closely balances a mean surface rainfall per echo, and the net enthalpy source by the cumulonimbus system. Fluxes of θ_E into and out of the system for 5^oK ranges confirm energy conservation, and give updraft, downdraft transports. The vertical structure of net mass, r , θ_E fluxes are presented. The mesoscale results are related to the large-scale modification of the mean atmosphere, using a theoretical cumulonimbus model. The large scale vertical motion is computed as a residual from the temperature and water vapour budgets. Suitably averaged, the synoptical scale mass transport is similar but not identical to the (lifecycle mean) cumulonimbus vertical mass transport. It is concluded that parametric models of cumulonimbus convection in terms of mass transport are quite realistic for this data above the surface 150 mb, where the effects of horizontal variations between updraft and downdraft are dominant. The precise

relationship between synoptic scale controls and cumulonimbus scale mass transport remains unclear.

LIST OF TABLES

LIST OF FIGURES

1. INTRODUCTION

a) Outline of problem:

The vertical transports by deep convection (cumulonimbus convection) present a formidable problem to the understanding and modelling of the tropical atmosphere. The releases of latent heat are large, and the vertical redistribution of enthalpy and water vapor is very significant in determining the structure and time development of the mean atmosphere. However, deep convection can also be regarded as a response to the large-scale thermodynamic fields, which in turn result from the large-scale horizontal and vertical motion fields. Deep convection is one major process by which the atmosphere maintains an equilibrium structure which in some sense is stable. The resulting large-scale mean field is a subtle balance between large-scale forcing, (e.g. mean vertical motion) and convective heat inputs and transports. Changes in the mean atmosphere structure are thus smaller residuals of two larger opposing terms. Since we require these net changes, the details of the cumulonimbus induced changes must be well understood. This is not an easy task, theoretically or observationally.

b) Objective of this study:

This work is directed to the observational problem, although the theoretical interpretation of the data is also discussed. To obtain an 4-D data set on the mesoscale (10-100Km), adequate to resolve the structure and time development of a cumulonimbus system, still seems impracticable with present techniques. During experiment VIMHEX (Venezuelan International Meteorological and Hydrological Experiment; 1969; director: H. Riehl) an attempt was made to deduce a mean structure for a mesoscale cumulonimbus system (area > 400 km^2) using the simplest

possible technique: one 10 cm radar, and a single rawinsonde station. The results, discussed in this paper, were encouraging. By carefully compositing data from many different days and storms, it was possible to construct maps for the flow into and around a mean storm at all pressure levels from the surface to above the outflow for both the growth and decay phases. Budget calculations on this mean system will be presented, and interpreted on the synoptic scale.

2. DATA COLLECTION AND ANALYSIS

a) Radar

A modified M-33 10 cm radar was located at Anaco in north-eastern Venezuela for four months, June to September 1969. The radar was scanned at successive elevation increments of 2^{o} to its maximum elevation angle of 18^{o}, and the P.P.I. display was photographed with a 35 mm camera at attenuations of 0, 6, 12, 18 db. This sequence of operations was repeated approximately every 15 mins when echos were visible. Using a microfilm reader, positions of major echos were traced, and echo area and heights calculated. Only systems which reached a maximum area greater than 400 km^2 were used to construct composites. The definition of a mesoscale system, often clusters of smaller cumulonimbus cells, clearly introduces some subjectivity: the radar analysis is discussed further in Cruz (1972). A mean velocity vector of an echo was calculated from the beginning and end of the trajectory (though for a few longer lasting storms, where wind-field and motion vector seemed to change appreciably during their lifetime, mean tracks for shorter periods were calculated). From the time sequence of echo area and height, a growth and decay phase for each echo could be defined with little ambiguity. Statistics for the mean echo were computed from a total of about 230 echos for the experiment period (Cruz, 1972). Some of these are shown in Table 1.

TABLE 1. MEAN ECHO STATISTICS

Mean echo radius	$R = 12.5$ km
Mean echo growth time	$\tau = 66$ mins
Mean echo decay time	$\tau = 66$ mins
Mean echo travel speed	$= 7$ ms^{-1}

The mean echo area (A_o) was taken as 500 km^2, the area (A_R) scanned by the radar (working radius 80 km) was taken as 20,000 km^2.

b) Rawinsonde

Before, during, and after the period of deep convective activity, rawinsonde ascents were made adjacent to the radar at a time frequency initially of two hours, and later in the experiment only one hour. The strip chart data was tabulated at one minute intervals and interpolated to specified pressure levels (at 25 or 50 mb intervals). It was found that the hygristor (Type ML-476) suffered from serious error in direct sunshine (see e.g. Morrissey and Brousaides, 1970), and some correction was essential. A temperature difference independent of height between hygristor and thermistor was assumed, and a value deduced by comparing the surface relative humidity recorded by the radiosonde (extrapolated where necessary) with an accurate surface value obtained simultaneously with an aspirated psychrometer. This simple correction eliminates the major systematic error in the lowest levels - further details are indicated in the Appendix. Fortunately about half the data obtained during disturbed conditions were after sunset or under stratiform cloud, when the hygristor error is relatively small. Humidity values obtained before the period of deep convection under strong sunshine are less reliable as the correction is large (~ 4g/Kg).

c) Construction of composite

The balloon position relative to a storm was calculated for each pressure level, and the co-ordinate system of each observation rotated so that all storm motion vectors were aligned along the positive X axis. The distance of the rawinsonde to the echo was also scaled by an echo radius measured along the line to the rawinsonde. The result of this simple scaling is that with echo radius unity, all data points

within the unit circle were taken within the radar echo, while those at greater radii were outside the echo. Some scaling of distance is essential to compensate for different echo sizes: the procedure used here does not preserve divergence, but was chosen for simplicity. Wind velocities (V_r) relative to the storm were calculated by subtracting the storm mean velocity vector at all levels, and maps were plotted of V_r, equivalent potential temperature θ_E, mixing ratio r, and a temperature perturbation T', at pressure levels of 950, 900, 850, 800, 700, 600, 500, 400, 300, 250, 200, 175, 150 mb. The temperature perturbation was defined near the surface (850 to 950 mb) as the difference between the deviation from the morning (0800) sounding, and a mean diurnal curve (with zero also at 0800) constructed from all the soundings. At higher levels a simple temperature difference from the last sounding preceding the onset of deep convection was taken. This apparently elaborate procedure is necessary since the synoptic and, at low levels, diurnal temperature variations are as large as the changes produced locally by the convection. Indeed the two can only be partially resolved. Humidity perturbation maps were not constructed because the water vapor measurements were of less basic accuracy owing to the poorly ventilated and radiation-shielded hygristor. Composite maps were constructed for the growth and decay phases of a mean system for specific synoptic classifications.

d) Synoptic classification

To construct a composite mesoscale wind field around a cumulonimbus system, it is necessary for the synoptic scale wind fields of different days to be comparable. Three attempts at classification using the synoptic wind fields over Venezuela and the Caribbean, at 850 and 200

mb, were made

(i) By thermal structure: thickness 850 to 200 mb: warm or cold core.

(ii) By vorticity difference: 850 to 200 mb.

(iii) By 850 and 200 mb winds relative to mean echo motion for that day.

The third classification was most successful; the others are less closely related to the wind field relative to an echo. Composite maps were therefore constructed for days with comparable high and low level synoptic scale wind fields relative to a mean storm motion vector for that day.

Only one synoptic class proved to have a large enough data sample for analysis: that in which the low level flow was easterly, the storms moved westward faster than the low level flow, and the upper level flow has a westerly component. In the frame where the storm is stationary, the relative wind-field is nearly two-dimensional, with flow in the front at low levels, and out to the rear at outflow levels ($\sim$ 175 mb).

Important data characteristics for this class of days are shown in Table 2.

TABLE 2. DATA FOR DAYS IN COMPOSITE ANALYSIS

No. of days	17
Total no. of echos	90
Total mean rainfall in echo area	101 mm
Mean rainfall/day	5.9 mm
No. of echos/day N =	5.3
Mean rain period/day Δt =	6.7 hrs

e) Composite analysis

The mixing ratio, equivalent potential temperature, temperature perturbation, and streamline fields were analyzed at each level for the growth and decay phases. A full isotach analysis seemed less convincing, and in the light of the theoretical framework discussed in the next section, it was decided that only fluxes into and out of the echo could be calculated to useful accuracy.

The mean echo was considered enclosed in a cylindrical shell from surface (990 mb) to 137.5 mb (see Fig. 1), non-dimensional radius $\hat{R} = 2$ ($\hat{RR}$ = radius vector from mean storm center). Fluxes across the vertical boundary of this cylinder were computed at the pressure levels from 950 to 150 mb: net vertical mass flux at 137.5 mb proved negligible. Examples of the analysed fields are shown in Figs. 2a, 2b.

Mass flux. Wind speeds were estimated from the rather scattered data at 12 equally spaced intervals on the circle $\hat{R} = 2$. Radial velocities C_k ($k = 1, 12$) were calculated from wind speed and streamlines. Though the scatter in the individual data was considerable, the resulting net mass convergence varied uniformly with pressure (though in opposite senses) for growth and decay phases. Little reanalysis was necessary.

Water vapor, and temperature perturbation. The mass convergence analysis was overlaid in turn on the analyzed fields of water vapor and temperature perturbation.

Net fluxes into the echo across the circle $\hat{R} = 2$ were calculated using the 12 values of C_k and corresponding means r_k, T'_k for r', T', for each circumference interval.

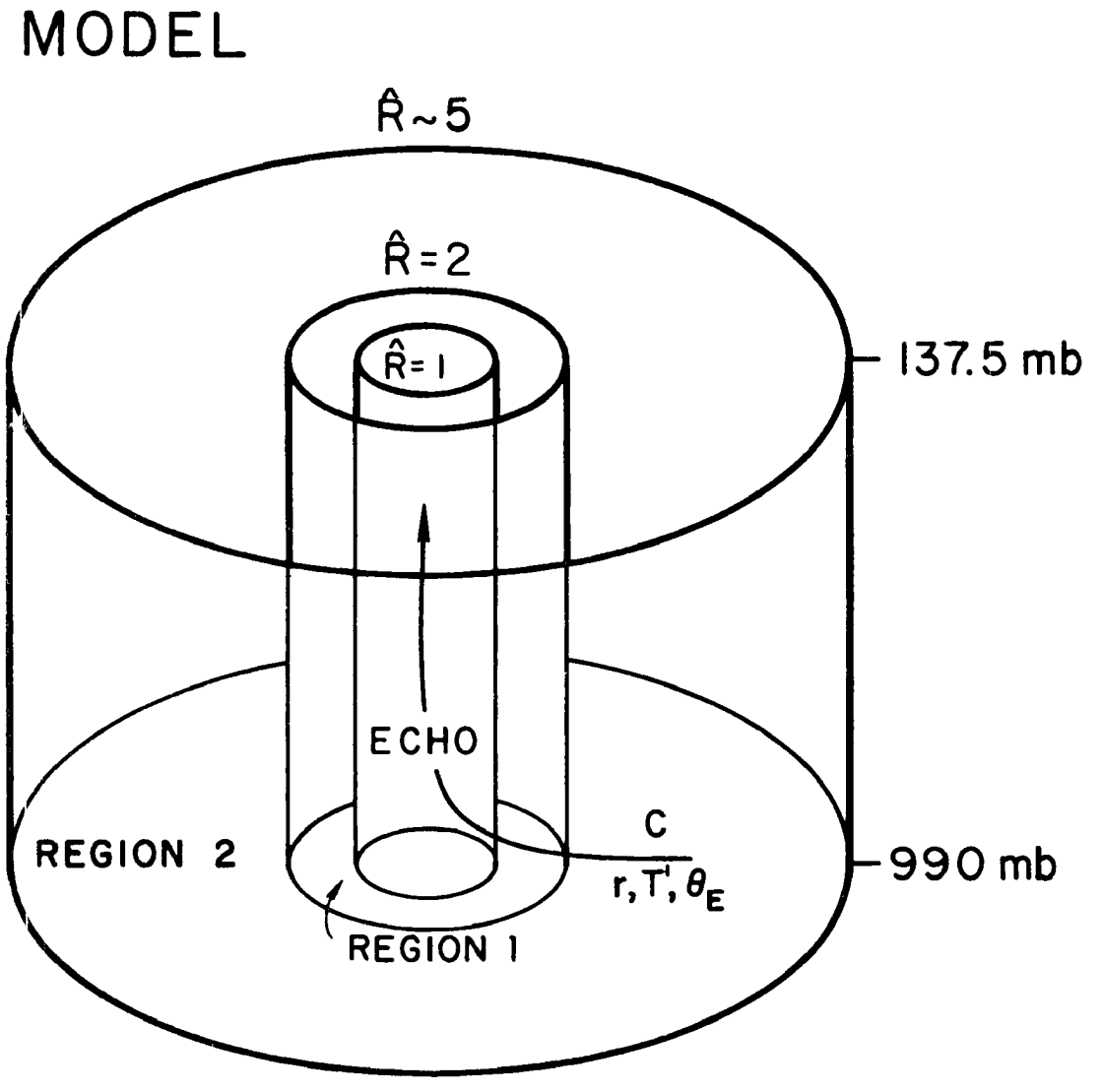

Figure 1. Sketch of cumulonimbus model used for budget computations.

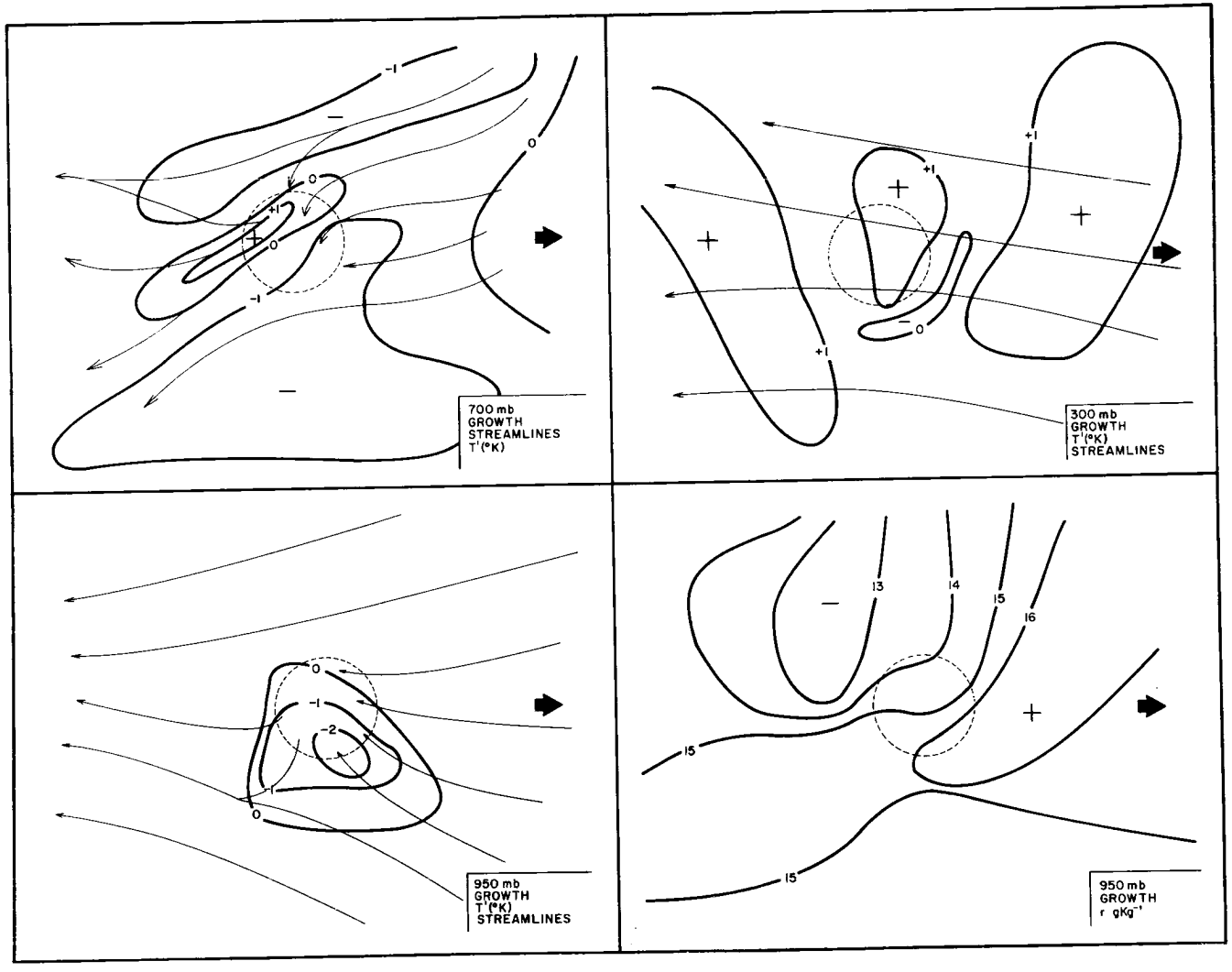

Figure 2a. Example mesoscale fields around mean echo (diameter 25 km) at 950 mb, 700 mb, and 300 mb (growth).

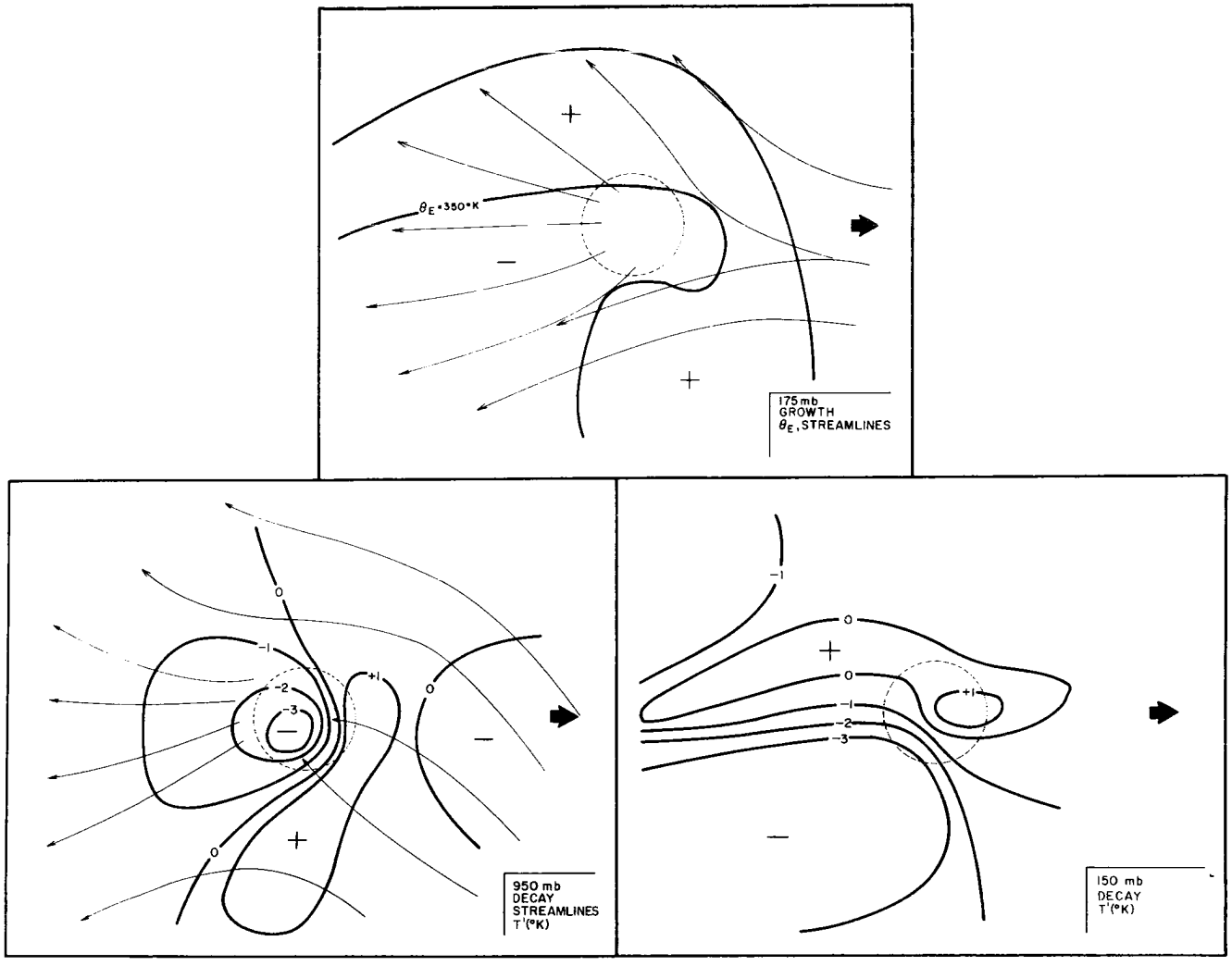

Figure 2b. Example mesoscale fields around mean echo (diameter 25 km) at 175 mb (growth), 950 mb and 150 mb (decay).

Equivalent potential temperature. The field of θ_E was treated differently from those of r , T . In a precipitating system, the release of latent heat resulting from a net condensation of water vapor to liquid, increases the enthalpy of the mean atmosphere. A budget on a cumulonimbus system may be regarded as conserving enthalpy plus latent heat on a scale of an hour or two.

It is convenient to use θ_E as a conserved quantity both to investigate this energy conservation, and to give a more detailed picture of the vertical transports (Rasmussen et al. 1969). The usual definitions of θ_E involve approximations (e.g., neglect of specific heat of liquid water), the ice phase is not considered, and in isobaric mixing $\int C_p \theta_E \rho dV$ is only approximately conserved (see e.g., Betts 1970). However typical errors are about 5% and within the level of accuracy of this experiment.

The convergence analysis was overlaid on the θ_E analysis and the net mass flux in 5^oK ranges of θ_E (from $330\text{-}355^oK$) into the composite system was calculated.

f) Mean fields

The theoretical framework presented in the next section requires averages of T , r etc., outside the volume containing the echo. These were calculated as simple averages of the data values outside $\hat{R} = 2$. More data points would be preferable to obtain a representative average, but this average is not critical. More critical are representative synoptic scale averages of T , r before and after the period of deep convection, which are essential to interrelate mesoscale transports and the synoptic scale motion field (section 3). Mean values $\overline{T}(p)$ for the 17 days on the data set (Table 2) were obtained by

averaging the last soundings preceding the deep convection, and the soundings immediately afterwards. The mean horizontal advection over these 17 days will be supposed negligible for the large-scale budget calculations.

Representative values of $\overline{T}(p)$ near the surface (990-850 mb) were not thought obtainable because of the large diurnal temperature change, and the widely varying time interval between the last sounding preceding the rain period, and the rain period itself.

Mean values $\overline{r}(p)$ after the deep convection, were found similarly, but a mean sounding before could only be obtained by selecting from a much larger sample, owing to the serious inaccuracies in the humidity sensor. The humidity errors are largest prior to a rain episode when solar radiation is large and cloud cover relatively small. The synoptic scale r budget is thus only indicative.

3. THEORETICAL MODEL

a) Model description

The mean echo was considered enclosed in a cylindrical shell from 990 mb (the surface) to 137.5 mb, radius $\hat{R} = 2$ ($\hat{R} = 1$ corresponds to mean echo -- see Fig. 1). The region inside the cylinder, the cloud region, will be labelled region 1; outside, the environment, will be labelled region 2. The fluxes into the cylinder across the 1, 2 boundary were measured at pressure levels from 950-150 mb (sections 2(e), 5), and the net vertical mass flux at 137.5 mb proved negligible (section 5(a)). The area ratio of regions 1 to 2 is a time-space average and is discussed later in 4(e). This model of cumulonimbus convection is an extension of those of Pearce and Riehl (1968) and Yanai (1971).

In region 2, potential temperature and water vapor will be considered conserved, that is, all the phase changes of water will be supposed to take place in region 1 (an area four times the mean echo area). Radiative fluxes have been omitted, since they are sensitive functions of a largely unknown distribution of cloud. Though not necessarily negligible, they are considerably smaller than the cumulonimbus heating on the measured time scale of 1-6 hours.

b) Conservation equations

For a conserved property Q

$$\frac{\partial}{\partial t}(\rho Q) + \nabla\cdot(\rho \mathbf{V} Q) = 0 \qquad (3.1)$$

Eq. 3.1 can be integrated over both regions. Certain assumptions will be made in the budget equations:

$\rho = \rho(p)$ only

$p = p(z)$ only (hydrostatic assumption)

and a density weighted vertical velocity will be defined as

$$\omega = -\rho g w \quad .$$

Over region 1, after horizontal averaging and using the divergence theorem

$$A_1 \frac{\partial}{\partial t} \tilde{Q}^1 + A_1 \frac{\partial}{\partial p} \widetilde{\omega Q}^1 + \int_{\ell_1} CQ d\ell_1 = 0$$

where ℓ_1 is the length of the 1, 2 boundary

C is the radial component of the horizontal wind.

(positive outwards)

This will only be used in region 1 for mass, for which $Q = 1$

$$\frac{\partial}{\partial p} \tilde{\omega}^1 = - \frac{1}{A_1} \int_{\ell_1} C d\ell_1 \tag{3.2}$$

$$\therefore A_1 \tilde{\omega}^1 = - A_1 \rho g \tilde{w}^1 = - \int_{990}^{137.5} dp \int_{\ell_1} C d\ell_1 \tag{3.3}$$

with the boundary condition $\tilde{w}^1 = 0$ at $p = 990$ mb . $A_1 \tilde{\omega}^1$ is a cumulonimbus scale mass transport.

Over region 2

$$A_2 \frac{\partial}{\partial t} \tilde{Q}^2 + A_2 \frac{\partial}{\partial p} \widetilde{\omega Q}^2 - \int_{\ell_1} CQ d\ell_1 + \int_{\ell_2} CQ d\ell_2 = 0 \tag{3.4}$$

For mass, $Q = 1$, and 3.4 reduces to

$$\frac{\partial \tilde{\omega}^2}{\partial p} = - \frac{A_1}{A_2} \frac{\partial \tilde{\omega}^1}{\partial p} + \frac{A_1 + A_2}{A_2} \frac{\partial \tilde{\omega}}{\partial p}$$

where $\tilde{\omega}$ is a large-scale average over both cloud and environment,

related to the mass inflow across ℓ_2 , the length of the outer boundary of region 2.

Integrating, with $\tilde{\omega}^1 = \tilde{\omega}^2 = \tilde{\omega} = 0$ at p = 990 mb

$$\tilde{\omega}^2 = \frac{A_1+A_2}{A_2}\tilde{\omega} - \frac{A_1}{A_2}\tilde{\omega}^1 \qquad (3.5)$$

For $A_1 << A_2$ we note

$$\tilde{\omega}^2 = \tilde{\omega} - f\tilde{\omega}^1$$

where f is the fractional area cover of A_1 . The composite proceedure measures $\tilde{\omega}^1$, and this is being taken as representative of the cloud mass circulation. An alternative definition exists: that of defining $\tilde{\omega}^1 - \tilde{\omega}$ (the excess vertical mass flux over $\tilde{\omega}$ in region 1) as a measure of the cloud mass circulation. However, it could be argued that the latent heat release is related to $\tilde{\omega}^1$, rather than $\tilde{\omega}^1 - \tilde{\omega}$: the difference is of course small, since $\tilde{\omega} << \tilde{\omega}^1$.

For other properties $Q = \theta$, r , θ_E ; two further assumptions will be made to simplify 3.4. We shall assume no vertical eddy transport in region 2 (the environment)

$$\overbrace{\omega' Q'}^{2} = 0$$

a necessary approximation as we have no data on these transports. Clearly the vertical eddy transports outside the cloud region are likely to be much smaller than inside, and the data shows that fluxes across the 1-2 boundary are nearly in hydrostatic balance, at least above a surface layer. We shall also neglect large-scale horizontal gradients, and hence local changes by advection, by assuming $Q = \tilde{Q}^2$ on the outer

boundary ℓ_2 . 3.4 then simplifies to

$$A_2 \frac{\partial}{\partial t} \tilde{Q}^2 + A_2 \tilde{\omega}^2 \frac{\partial \tilde{Q}^2}{\partial p} - \int_{\ell_1} C \ (Q-\tilde{Q}^2) d\ell_1 = 0 \qquad (3.6)$$

The last term includes an 'eddy' flux across the 1-2 boundary through the correlation of C and Q . (If $Q = \tilde{Q}^2$ on the 1-2 boundary, then the last term is zero.) Using 3.5

$$A_2 \frac{\partial}{\partial t} \tilde{Q}^2 = - \left[(A_1 + A_2) \ \tilde{\omega} - A_1 \tilde{\omega}^1\right] \frac{\partial \tilde{Q}^2}{\partial p} + \int_{\ell_1} C(Q-\tilde{Q}^2) d\ell_1 \qquad (3.7)$$

Both the right hand terms are essentially residuals, and are typically quite small. The data will show that, in the middle atmosphere where vertical motions are large, the first term (derived from $\tilde{\omega}^2$) is dominant, while at the surface and above the main outflow, the last term becomes dominant.

c) Further derivations

By integrating over a cloud-life cycle, one may suppose that the area mean change is well approximated by that in region 2, that is

$$\frac{\partial \tilde{Q}^2}{\partial t} = \frac{\partial \tilde{Q}}{\partial t} \qquad (3.8)$$

This is valid if

$$\frac{A_1}{A_1+A_2} \frac{\partial}{\partial t} (\tilde{Q}^1 - \tilde{Q}^2) \ll \frac{\partial}{\partial t} \tilde{Q}^2$$

which is likely to be a reasonable approximation for $A_1/A_1+A_2 \sim 10\%$. However, this may be a better approximation for θ (as the atmosphere is never far from hydrostatic balance), than for r . Using the rawinsonde data of this experiment, $\tilde{Q}^2$ and $\tilde{Q}$ cannot be accurately distinguished, either in their time or pressure derivatives. Using

3.8, 3.7 becomes

$$\frac{A_2}{A_1+A_2}\frac{\partial \tilde{Q}}{\partial t} = -\left[\tilde{\omega} - \frac{A_1}{A_1+A_2}\tilde{\omega}^1\right]\frac{\partial \tilde{Q}^2}{\partial p} + \frac{1}{A_1+A_2}\int_{\ell_1} C(Q-\tilde{Q}^2)\,d\ell_1 \qquad (3.9)$$

The factor A_2/A_1+A_2 in 3.9 is close to unity, and quantitatively rather trivial. It arises from the inclusion in $\tilde{\omega}^1$ of the large-scale $\tilde{\omega}$ over the area A_1 .

One further transformation of 3.7 is important. Integrating over pressure, using 3.2, we note

$$\int_{990}^{137.5} dp\, A_1\tilde{\omega}^1\frac{\partial \tilde{Q}^2}{\partial p} - \int_{\ell_1} C\tilde{Q}^2 d\ell_1 = A_1\left[\tilde{\omega}^1\tilde{Q}^2\right]_{990}^{137.5} = 0$$

$$\therefore \frac{A_2}{A_1+A_2}\int_{990}^{137.5}\frac{\partial \tilde{Q}^2}{\partial t}\,dp = -\int_{990}^{137.5}\tilde{\omega}\frac{\partial \tilde{Q}^2}{\partial p}\,dp + \frac{1}{A_1+A_2}\int_{990}^{137.5} dp\int_{\ell_1} CQ\,d\ell_1 \qquad (3.10)$$

The pressure integrated modification outside the echo region may be expressed in terms of a large-scale term, and an exchange with the echo region, where Q may not be conserved. If $Q = \theta$, the last term represents a large input, since the mass divergence is at a higher θ , than the convergence.

If $Q = r$, this term is a large sink of water vapor, which falls out as rain, if there is no change in storage inside region 1.

If $Q = \theta_E$ then the last term is zero to the extent that θ_E integrated over mass is conserved in the wet process. Thus the pressure integrated local mean change of θ_E can be calculated from the large-scale $\tilde{\omega}$.

It should be stressed that 3.7 (or 3.8) is the equation for computing local changes at a pressure level: not the terms under the pressure integral on the right hand side of 3.10.

4. EVALUATION

a) Mass

3.3 was evaluated using 12 values of C, equally spaced on the circumference ℓ_1 at $\hat{R} = 2$ (see 2(e)), and pressure increments Δp between the halfway points between pressure levels. A few pressure increments have therefore uncentered values, but the data accuracy does not warrent an interpolation scheme. Vertical fluxes were computed using echo area A_o ($= A_1/4$) as a standard area, rather than A_1 (the inner cylinder cross-section). This does not affect the integrated vertical transport in region 1, and was done on the basis that the bulk of the vertical transport is probably within the echo, and vertical velocities so computed are more illuminating than if based on the arbitrary cylinder at $\hat{R} = 2$

$$A_o \omega^* = A_1 \bar{\omega}^1 \tag{4.1}$$

where $A_o = A_1/4$.

The theoretical model is now applied to the composite data: the overbar represents this composite mean; a 17 day mean (see Table 2) as well as an areal mean.

$$-\omega^* (p_i) = \frac{1}{3R} \sum_{i=1}^{i} \Delta p_i \sum_{k=i}^{12} C_k \tag{4.2}$$

since the increment of circumference $\Delta\ell = 4\pi R/12$

and chosen reference area $= \pi R^2$

In the tabulations and graphs, values of ΣC_k and ω^* for the growth and decay phases, which had <u>equal</u> duration, will simply be added to give the total life-cycle transport. This means that the reference time period for computing the total transport by the composite system over its life-cycle is the half lifetime: $\tau = 66$ mins (Table 1).

b) Water vapor

The convergence of water vapor (see 2(e)) into the system at a level is

$$\frac{\pi R\tau}{3g} \Delta p_i \sum_L \sum_k C_k r_k \tag{4.4}$$

where $\sum_L$ is to be interpreted as summing over the lifetime: that is, growth and decay phases.

c) Equivalent potential temperature

The vertical velocity was computed for each $5^{\circ}K$ range of θ_E: $\Delta\theta_{Ej}$.

$$-\omega^* (p_i, \Delta\theta_{Ej}) = \frac{1}{3R} \sum_L \sum_i \Delta p_i \sum_k C_k \, (\Delta\theta_{Ej}) \tag{4.5}$$

d) Temperature

Fields of temperature perturbation rather than potential temperature were plotted (see 2(c)). Letting Q be θ in 3.9, reexpressing in terms of T , T' , and finite difference form, one obtains (using 4.1)

$$\frac{A_2}{A_1+A_2} \frac{\partial}{\partial t} \overline{T}(p_i) = -\left[\overline{\omega} - \frac{A_o}{A_1+A_2} \omega^*(p_i)\right] \left[\frac{\overline{T}}{\overline{\theta}} \frac{\Delta\theta}{\Delta p}\right]_i + \frac{\Delta\ell}{A_1+A_2} \sum_k C_k (T_k' - \overline{T'^2}) \tag{4.6}$$

where $A_o = \pi R^2$, $\Delta\ell = \pi R/3$.

Of importance is the total enthalpy input by an echo

$$\frac{\tau}{g} \sum_L \left[- \pi R^2 \sum_i \Delta p_i \, \omega^*(p_i) \left(\frac{\overline{T}}{\overline{\theta}} \frac{\Delta\theta}{\Delta p}\right)_i - \frac{\pi R}{3} \sum_i \Delta p_i \sum_k C_k (T_k' - \overline{T'^2}) \right] \tag{4.7}$$

which will be compared to a latent heat release equivalent to the net vapor inflow into the system, (4.4).

e) Meso-synoptic interaction

The modification of the mean atmosphere over the entire period of deep convection is a time integration of 4.6 for the period Δt (Table 2).

$$\frac{A_2}{A_1+A_2}\,\Delta\bar{T}(p_i) = -\frac{\bar{T}}{\bar{\theta}}\frac{\Delta\theta}{\Delta p}\left[\bar{\omega}\Delta t - \frac{A_o}{2(A_1+A_2)}\,\Delta t \sum_L \omega^*\right] + \frac{\Delta t\,\Delta\ell}{2(A_1+A_2)} \sum_L \sum_k C_k(T_k' - \overline{T'^2}) \tag{4.8}$$

The area unit (A_1+A_2) per storm can be calculated (Table 2) from

A_R - the radar area

N - the number of echos/time period Δt in A_R

2τ - echo lifetime

$$(A_1+A_2) = A_R\,\frac{\Delta t}{2N\tau} = A_R/n \tag{4.9}$$

where n is the mean number of echos visible in A_R at one time. So one obtains

$$\frac{A_2}{A_1+A_2}\,\Delta\bar{T}(p_i) = -\frac{\bar{T}}{\bar{\theta}}\frac{\Delta\theta}{\Delta p}\left[\bar{\omega}\Delta t - \frac{A_o}{A_R}\,N\tau \sum_L \omega^*\right] + \frac{N\tau\,\Delta\ell}{A_R} \sum_L \sum_k C_k(T_k' - \overline{T'^2}) \tag{4.10}$$

Note that both time and space averages are involved in comparing ω^* with $\tilde{\omega}$. Within the observed area A_R, the mean fraction covered by echo at one time is

$$\frac{2N\tau}{\Delta t}\,\frac{A_o}{A_R} \approx 4\%$$

but over the daily period of convection, Δt, the total area 'covered' is

$$\frac{NA_o}{A_R} \approx 13\%$$

The analog of 4.10 for water vapor is

$$\frac{A_2}{A_1+A_2}\,\Delta\bar{r}(p_i) = -\frac{\Delta r}{\Delta p}\left[\bar{\omega}\Delta t - \frac{A_o}{A_R}\,N\tau \sum_L \omega^*\right] + \frac{N\tau\Delta\ell}{A_R}\sum_L\sum_k C_k(r_k - \bar{r}^2) \tag{4.11}$$

5. RESULTS

a) Mass budget

The convergence and divergence as a function of pressure for the growth and decay phases, and their sum (representing the net convergence) are presented in Fig. 3 and Table 3, and the vertical mass flux curves in Fig. 4. Neither growth nor decay phases show strict mass balance, but the difference is within experimental error. However, there is no reason why, using this composite technique, that one must obtain mass balance for each phase, since the sampling method is not instantaneous, and the phenomena is transient. For example, the growth phase lasted in the mean about 60 mins, the ascent time of an air parcel through a cumulonimbus at 10 ms^{-1} is about 20 mins, and the rawinsonde ascent time is about 50 mins. Thus sampling of the outflow at high levels may be some 30 mins later than the sampling of the corresponding inflow at low levels, though in fact the same rawinsonde rarely if ever samples both.

Since the growth and decay phases lasted equal times (Table 1), the sum of their mass transports is the best estimate of the net transport over the lifecycle of the system. This net mass budget shows mass balance, which simplifies the subsequent analysis. Though the net mass transport on the cumulonimbus scale is up at all levels, there is more structure than that corresponding to simple inflow at low levels and outflow at high levels. Referring to 4.6 it is clear that the decrease of the net ω^* from 800 to 600 mb will have important consequences on the synoptic scale modification of the atmosphere, unless $\bar{\omega}$ has a corresponding profile.

TABLE 4. NET θ_E BALANCE IN 5°K RANGES

(Sum of Growth and Decay Phases)

		θ_E RANGES (°K)											
p	(-Δp)	330-335		335-340		340-345		345-350		350-355		(330-345)	(345-355)
mb	mb	ΣC_k	(-ω*)	ΣC_k	(-ω*)	ΣC_k	(-ω*)	ΣC_k	(-ω*)	ΣC_k	(-ω*)	(-ω*)	(-ω*)
			0		0		0		0		0	0	0
950	65			11.5		25.2		-30.2		-21.7			
					-20		-44		52		38	-64	90
900	50			13.5		-17.8		- 7.4		- 3.7			
			0		-38		-20		62		43	-58	105
850	50	21.5		- 8.7		-15.4		- 2.1					
			-29		-26		1		65			-55	108
800	75	-6.2		0.4		9.8							
			-16		-27		-19					-63	108
700	100	11.6		- 0.9		- 8.5							
			-47		-25		4					-68	108
600	100	-11.7		9.8									
			-16		-51		4					-63	108
500	100	-4.2		1.7		- 1.8							
			-5		-55		8					-52	108
400	100			-13.1		- 4.7							
					-20		21					-4	108
300	75					-3.4							
							28					3	108
250	50					16.2		- 1.6					
							6		67			-19	110
200	37.5							32.4					
									35				77
175	25							41.7		32.0			
									7		21		28
150	25									14.1			
(Residual)			-5		-20		6		7		12	-19	19

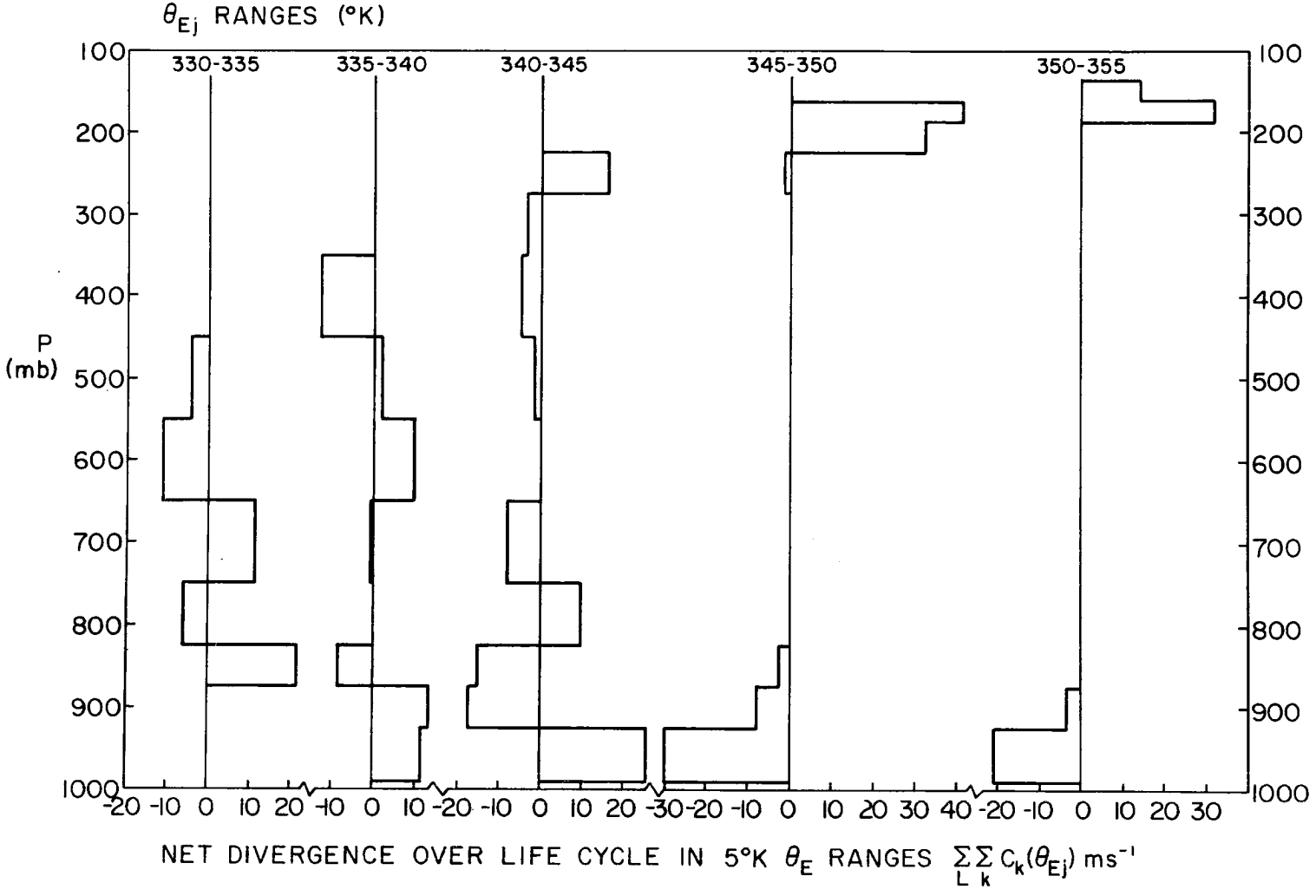

Figure 5. Graph of net lifecycle convergence into echo region 1 against pressure for 5° K θ_E ranges.

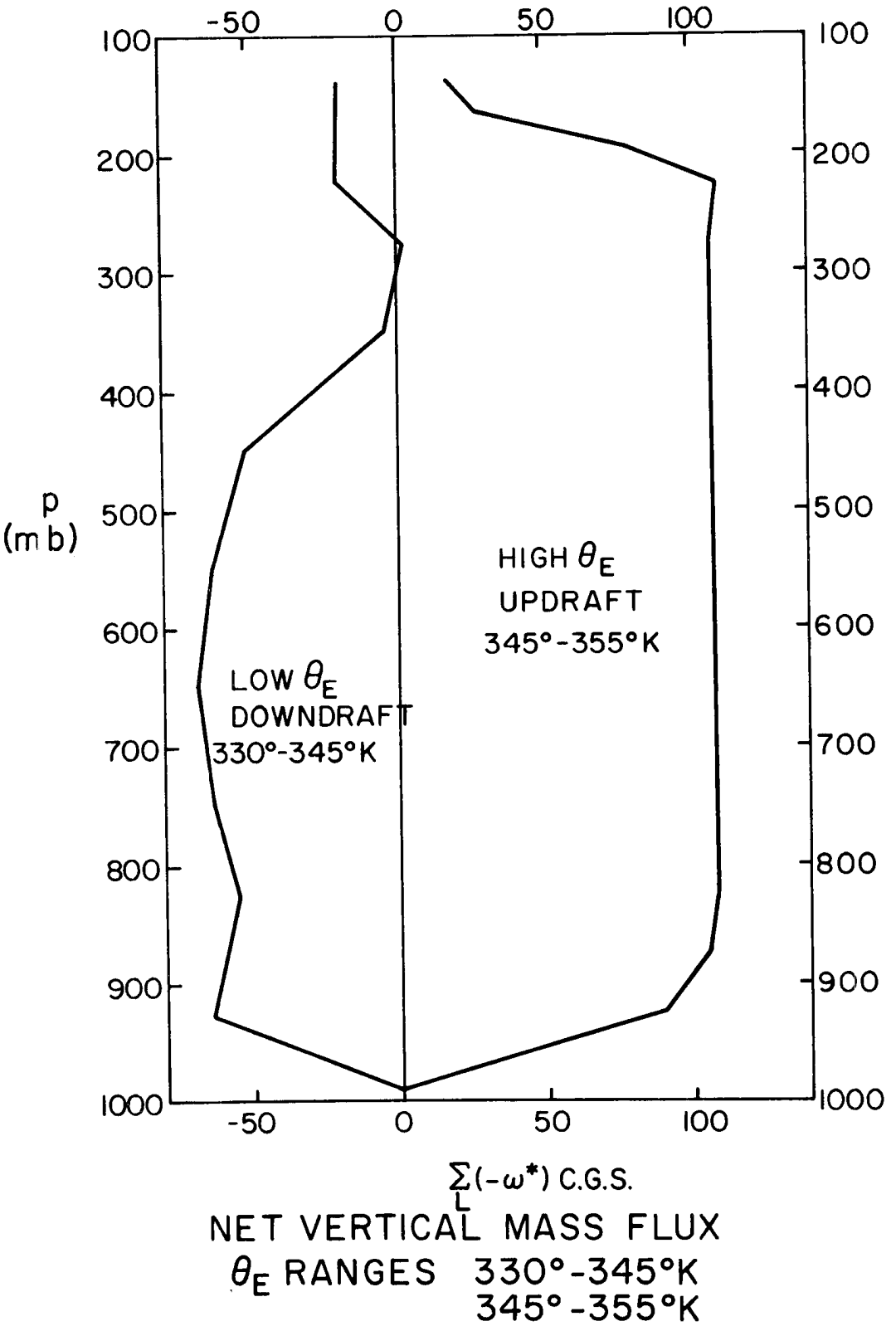

Figure 6. Graph of net vertical mass flux against pressure for high θ_E (345-355° K) and low θ_E (330-345° K) ranges, depicting simplified updraft and downdraft.

confirmed by the energy balance presented in the next section. The analysis of T', r, θ_E were however made independently, so some differences must be expected.

c) Water vapor, rainfall and energy conservation

The fluxes of water vapor into region 1 are shown in Table 5. The net vapor convergence into the system over the lifecycle will be taken to equal the rainfall. This requires some justification. It is not being said that all the water condensed falls as rain, only that which is not re-evaporated in downdrafts. By taking the θ_E ranges 330-345^oK and 345-355^oK, one can distinguish updraft condensation and downdraft evaporation more closely. These are also given in Table 5, where the net convergence into ascending 'hot towers', a measure of the total condensation, is about twice the vapor divergence from the lower θ_E downdrafts; a measure of the re-evaporation.

The total enthalpy input (Eq. 4.7) by the cumulonimbus system can be calculated from the thermal fields, and compared with the net latent heat release if the net vapor convergence is condensed (i.e., no change in vapor storage in region 1). This is tabulated in Table 6. The agreement is to a few percent, well within experimental error. Clearly the net condensation in region 1 only equals the rainfall if there is also no change in storage of liquid water from growth to decay phase. There were no measurements of the total mean liquid water content of the atmosphere, so this will be assumed.

The rainfall value equivalent to the net vapor convergence corresponds to 3.7 cm of rain over the echo area, during the echo lifetime.

TABLE 5. WATER VAPOUR BALANCE

	GROWTH			DECAY		SUM	
p	$(-\Delta p_i)$	$\Sigma C_k r_k$	$(\Delta p_i)\Sigma C_k r_k$	$\Sigma C_k r_k$	$(-\Delta p_i)\Sigma C_k r_k$	$\Sigma_L \Sigma C_k r_k$	$(-\Delta p_i)\Sigma_L \Sigma C_k r_k$
mb	mb	$ms^{-1} gKg^{-1}$	mb ms^{-1} gKg^{-1} x10		x10		x10
950	65	-452	-2808	168	1092	-264	-1716
900	50	-346	-1730	75	375	-271	-1355
850	50	-165	-825	83	415	-82	- 410
800	75	-66	-495	104	780	38	285
700	100	-57	-570	67	670	10	100
600	100	-49	-490	49	490	0	0
500	100	4	43	-16	-160	-12	- 117
400	100	0	0	-22	-220	-22	- 220
300	75	2	13	-4	-30	-2	-17
	$\Sigma_i(-\Delta p_i)\Sigma_k C_k r_k$		-6862		+3412	$\Sigma_i(-\Delta p_i)\Sigma_{Lk}\Sigma C_k r_k$	-3450
	Vapour convergence into updraft ($\theta_E > 345°$)			Vapour divergence from downdrafts ($\theta_E < 345°$)			Sum
			-6180		+2730		-3450
	Units x 10 mb ms^{-1} gKg^{-1}						

Key: (i) Net Vapour convergence = $\frac{\pi R \tau}{3g} \Sigma_{Li} \Sigma \Delta p_i \Sigma_k C_k r_k$

= $1.83\ 10^{13}$ gm water/echo

Over area $\pi R^2 \equiv$ 3.7 cm rain

TABLE 6. ENERGY CONSERVATION CHECK (Eq. 4.7)

p	$\overline{\theta}^2$ °K	$\Delta\overline{\theta}_i^2$ °K	$\Sigma_L(-\omega^*)$ c.g.s.	$\overline{\theta}/\overline{T}$	T_1	T_2	$T_1 + T_2$ 10 mb ms^{-1} °C
990	301.0						
950	301.2	0.8	13	1.01	41	325	-284
900	302.6	1.5	37	1.03	206	-260	-54
850	304.3	2.1	51	1.05	382	-275	107
800	306.7	3.7	49	1.07	634	75	709
700	311.6	5.8	43	1.11	840	0	840
600	318.4	7.2	43	1.16	1000	220	1220
500	325.9	7.4	51	1.22	1161	230	1391
400	333.3	7.5	80	1.30	1728	10	1738
300	340.8	5.1	107	1.41	1453	83	1536
250	343.5	3.0	101	1.49	761	-20	741
200	346.8	2.5	75	1.57	446	94	540
175	348.6	3.1	35	1.65	248	-23	225
150	353.0	(4.5)	5	1.72	49	-280	-231
					Σ 8949	-471	8478
				$\div L/c_p = 2.5$	3580	-190	3390
						6%	

Key (i) Total: 3390 Units is an enthalpy source to be compared with vapour convergence of -3450 units.

(ii) In 4.7 T_1 is $-3R\ \Delta p_i \sum_L \omega(p_i)\ \left(\frac{\overline{T}}{\overline{\theta}} \frac{\Delta\theta}{\Delta p}\right)_i$

T_2 is $-\Delta p_i \sum_L \sum_k C_k (T'_k - \overline{T}'^2)$

UNITS x 10 mb ms^{-1} °C

(iii) Enthalpy source is $\frac{\pi R\tau}{3g} C_p \sum_i (T_1 + T_2) = 1.08\ 10^{16}$ cals/echo

This can be compared with the measured mean rainfall per echo for the days in the data set (Table 2) calculated for the echo area.

Mean rainfall/echo =

$$\frac{101}{90} \times \frac{A_R}{A_o} = 4.5 \text{ cm}$$

This value is somewhat larger than the mesoscale budget value. The reason probably lies in the average values used for the mean echo (Table 1) for R , τ . There exist a size spectrum of echos (Cruz, 1972) with some correlation between larger radius and longer lifetime. From 4.4 the net vapor convergence is

$$\frac{\pi R\tau}{3g} \sum_i \Delta p_i \sum_L \sum_k C_k r_k \quad .$$

Over the whole data sample for the summer (about 230 echos)

$$\overline{R\tau} = 1.1 \, \overline{R} \, \overline{\tau} \tag{5.1}$$

so that the use of average values $\overline{R}$, $\overline{\tau}$ may underestimate total echo rainfall by 10%. The same data gave

$$\overline{R^2} = 1.1 \, \overline{R}^2 \tag{5.2}$$

so that the comparison figures of rain per unit echo area of 550 km^2 become

Budget	3.7 cm
Measured	4.1 cm

which agree within experimental error.

In this paper only simple mean values $\overline{R}, \overline{\tau}$ have been used, although clearly the correlation $\overline{R\tau}$ is important to the interpretation of composite budgets. This requires further study.

d) Large-scale modification

Mean values for $\Delta\overline{T}(p_i)$ in 4.10, for 800 mb and above, calculated for the 17 days used to construct the composite, are tabulated in Table 7, together with a mean sounding for region 2. No values for $\tilde{\omega}$ are known since the experimental site in Venezuela is not within a good synoptic network. However, it is illuminating to calculate a mean value (for the 17 days) for $\overline{\omega}$ using 4.10, while noting that 4.10 involves the assumption of no mean large scale changes due to horizontal advection. The computation is shown in Table 8; it uses the thermal cumulonimbus transports from Table 6. Two values for synoptic scale vertical motion are given: $\overline{\omega}$ which is a mean value for the time period Δt of deep convection, and $\overline{\omega}^*$ which is scaled to the area and half lifetime of the composite, so as to be directly comparable with $\Sigma\omega^*_L$. The maximum value of $\overline{\omega}$ is about -2 c.g.s. units which is not unreasonable. Values of $\overline{\omega}^*$ and $\Sigma\omega^*_L$ are plotted in Fig. 7. It is to be noted that $\overline{\omega}^*$ and $\Sigma\omega^*_L$ do not differ by much (see section 6).

The calculation was repeated using water vapor changes (Eq. 4.11) to give a second value of $\overline{\omega}^*$ (Tables 9, 10 and Fig. 7). As stated in 2(f) the water vapor changes Δr are not considered very reliable, but the values for $\overline{\omega}^*$ agree within the errors: except perhaps at 300-400 mb where the water vapor calculation gives rather larger values for $\overline{\omega}^*$. Evaporation from the surface may affect $\overline{\omega}_r$ at 950 mb.

The large scale $\overline{\omega}^*$ is larger than the cumulonimbus scale $\overline{\omega}^*$ between 700 and 300 mb. Thus the motion in region 2, the 'environment' is here upward, producing a cooling and moistening, although at 600 mb the lifting is small and cancelled by a lateral transport of enthalpy out of the cloud region 1.

TABLE 7. MEAN SOUNDINGS AND MEAN CHANGES OVER DEEP CONVECTIVE PERIOD

p mb	$\overline{T}^2$ °C	$\overline{r}^2$ gKg^{-1}	$\Delta\overline{T}$ °C	$\Delta\overline{r}$ gKg^{-1}
990	26.0	(17.0)	-	-
950	23.6	15.3	-	-0.3
900	20.4	13.7	-	-1.0
850	17.2	12.3	-	-0.8
800	14.5	10.6	0.4	-0.4
700	8.2	8.2	0	0
600	1.9	5.0	0	0.4
500	-6.0	2.7	-0.3	0.4
400	-16.8	1.2	-0.2	0.4
300	-31.8	0.3	0.2	0.15
250	-42.2	(0.1)	0.1	
200	-54.5		-0.3	
175	-61.5		-0.8	
150	-68.1		-1.3	

TABLE 8. SYNOPTIC SCALE $\bar{\omega}$ CALCULATION FROM $\Delta\bar{T}$ (eq. 4.10)

p	ΔT_{Cb} °K	$\frac{A_2 \Delta\bar{T}}{A_1 + A_2}$ °K	$\Delta T_{\bar{\omega}}$ °K	$-\frac{\bar{T}\Delta\theta}{\bar{\theta}\Delta p_1}$ °Kmb $\times 10^{-1}$	$(-\bar{\omega})_T$ c.g.s.	$(-\bar{\omega}^*)_T$ c.g.s.
950	-0.61					
900	-0.15					
850	0.30					
800	1.32	0.4	-0.9	0.46	0.81	37
700	1.18	0	-1.2	0.52	0.96	44
600	1.71	0	-1.7	0.62	1.14	52
500	1.95	-0.3	-2.2(5)	0.61	1.53	70
400	2.44	-0.2	-2.6(4)	0.58	1.88	87
300	2.88	+0.2	-2.7	0.48	2.34	107
250	2.08	+0.1	-2.0	0.40	2.08	95
200	2.02	-0.3	-2.3	0.42	2.28	104
175	1.26	-0.7	-2.0	0.75	1.11	51
150	-1.29	-1.1	-0.2	1.05	0.08	4

Key (i) ΔT_{Cb} is change in temperature induced by cumulonimbus convection in time Δt.

$$\Delta T_{Cb} = \frac{\pi R \tau}{3\Delta p_i} (T_1 + T_2)_i \frac{N}{A_R}$$ (see Table 6 (ii) for T_1, T_2)

(ii) $\Delta T_{\bar{\omega}} = -\frac{\bar{T}\Delta\theta}{\bar{\theta}\Delta p} \bar{\omega}\Delta t$ (see Table 2 for Δt, N)

(iii) $\frac{N\tau A_o}{\Delta t A_R} \bar{\omega}^* = \bar{\omega}$ where $\frac{N\tau A_o}{\Delta t A_R} = 0.022$ (Dimensionless)

This factor is the percentage of area covered at one time by clouds in, for example, the growth phase.

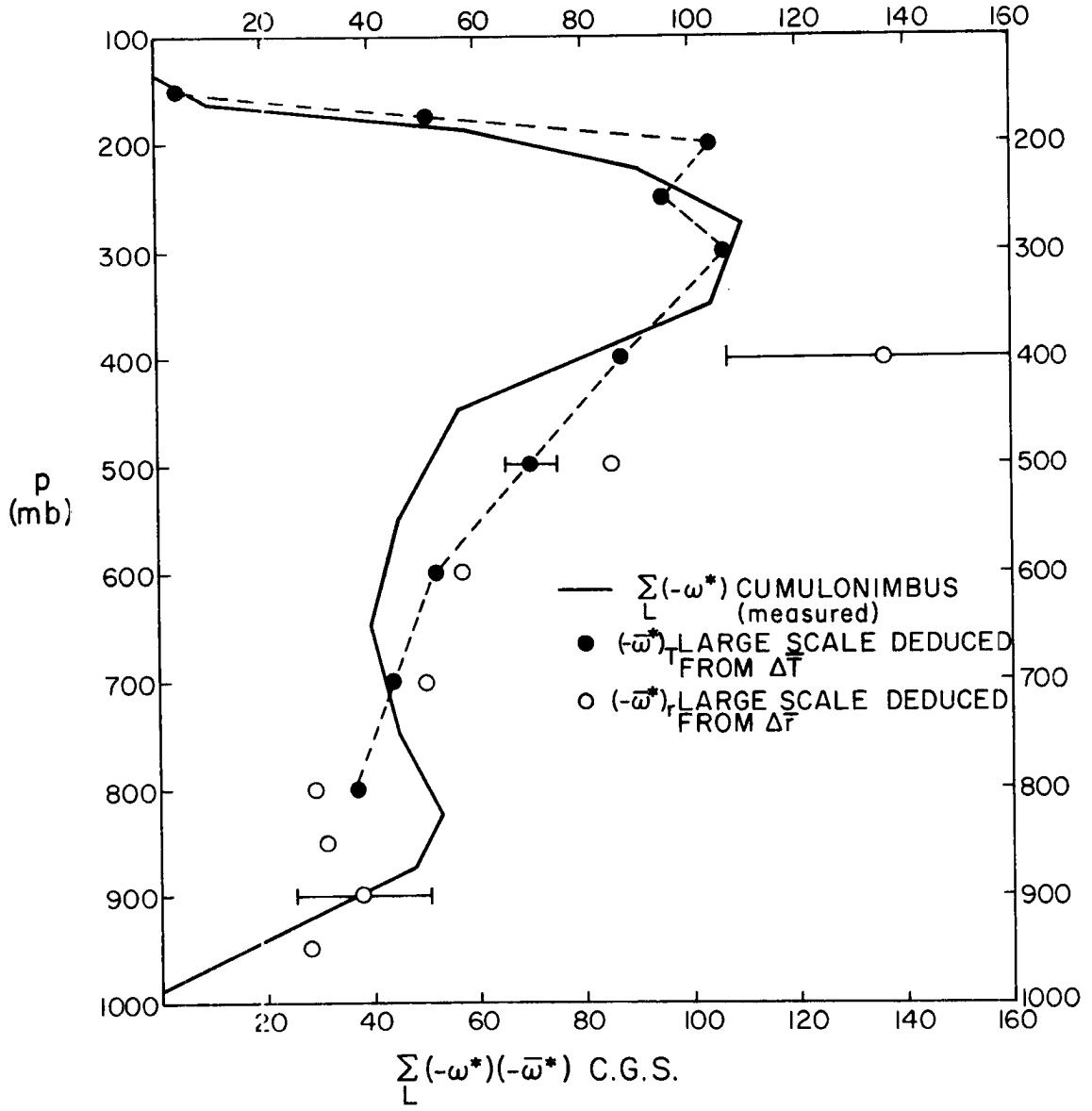

Figure 7. Graph of large-scale mean vertical mass flux, deduced from cumulonimbus budget and large-scale mean changes of temperature and mixing ratio. Error bars correspond to ±0.1°C in $\Delta\bar{T}$ and ±0.2 gKg^{-1} in $\Delta\bar{r}$.

TABLE 9. WATER VAPOUR MODIFICATION OF THE ATMOSPHERE

p mb	$\overline{r^2}$ gKg^{-1}	$\Delta\overline{r^2}_i$ gKg^{-1}	$\sum_L(-\omega^*)$ c.g.s.	R_1	R_2	R_1+R_2 10mb ms^{-1} $g\ Kg^{-1}$
990	(17.0)					
950	15.3	-1.7	13	-80	-210	-290
900	13.7	-1.5	37	-210	-300	-510
850	12.3	-1.6	51	-305	-120	-425
800	10.6	-2.0	49	-365	-30	-395
700	8.2	-2.8	43	-450	-80	-530
600	5.0	-2.7	43	-435	100	-335
500	2.7	-1.9	51	-365	0	-365
400	1.2	-1.2	80	-360	-10	-370
300	0.3	-0.5	107	-220	-10	-230
250	0.1					
				Σ -2790	-660	-3450
					19%	

Key (i) $R_1 = -3R\,\Delta p_i \sum_L \omega(p_i)\left(\frac{\Delta r}{\Delta p}\right)_i$

$R_2 = -\Delta p_i \sum_L \sum_k C_k(r_k - \overline{r^2})$

UNITS x 10mb ms^{-1} gKg^{-1}

TABLE 10. SYNOPTIC SCALE $\bar{\omega}$ CALCULATION FROM $\Delta\bar{r}$ (eq. 4.11)

p	Δr_{Cb}	$\frac{A_2\Delta\bar{r}}{A_1 + A_2}$	$\Delta r_{\bar{\omega}}$	$\Delta r/\Delta p$	$(-\bar{\omega})_r$	$(-\bar{\omega}^*)_r$
mb	gKg^{-1}	gKg^{-1}	gKg^{-1}	gKg^{-1}/100mb	c.g.s.	c.g.s.
950	-0.63	-0.25	0.38	2.62	0.60	28
900	-1.43	-0.84	0.59	3.00	0.82	38
850	-1.19	-0.67	0.52	3.20	0.67	31
800	-0.74	-0.34	0.40	2.67	0.62	29
700	-0.74	0	0.74	2.80	1.10	50
600	-0.47	0.34	0.81	2.70	1.24	57
500	-0.51	0.34	0.85	1.90	1.86	85
400	-0.52	0.34	0.86	1.20	2.98	136
300	-0.43	0.13	0.56	0.67	3.46	159

Key (i) Δr_{Cb} is change in mixing ratio induced by cumulonimbus convection in time Δt.

$$\Delta r_{Cb} = \frac{\pi R\tau}{3\Delta p_i} (R_1 + R_2)_i \frac{N}{A_R}$$ (see Table 9 (i) for R_1, R_2)

(ii) $\Delta r_{\bar{\omega}} = - \frac{\Delta r}{\Delta p} \bar{\omega} \Delta t$ (see Table 2 for Δt, N)

(iii) $\bar{\omega}$, $\bar{\omega}^*$ are related as in Table 8 (iii).

6. DISCUSSION AND CONCLUSIONS

a) Mass transport models

Simple parameterisations of deep convection involving vertical mass transport (Riehl and Malkus, 1958, Pearce and Riehl, 1963, Ooyama, 1969, Yanai, 1971) and lateral exchange (Kuo, 1965) can be examined using 3.9, 3.10, 4.10, 4.11 and Tables 6 and 9. Clearly the dominant terms are those in $\omega^* \partial\bar{\theta}/\partial z$ and $\omega^* \partial\bar{r}/\partial z$, the mass transport terms. For the heat balance the integrated 'lateral' term $(\Delta\ell \sum_L \sum_i \Delta p_i \sum_k C_k(T_k' - \bar{T}^2))$ represents only 6% (190/3390 in Table 6) of the total enthalpy input, a result of near hydrostatic balance. For water vapor the corresponding vapor term is rather larger, 19% (660/3450 in Table 9) of the total vapor convergence. Except for the surface levels 950-850 mb and at 150 mb, a simple mass transport model using ω^* and a mean atmosphere, correctly represents about 90% of the cumulonimbus scale modification. The total vapor convergence, calculated using $\bar{\omega}^*$ (from water vapor budget 850-950 mb and thermal budget above) and $\bar{r}^2$, is 2930 units to be compared with the total precipitation of 3450 units. Thus synoptic scale vapor convergence is fairly closely a measure of the heating of the atmosphere. With the mean sounding (Table 7) and the wet adiabat 350°K, Kuo's method gives a precipitation only about one quarter of the total vapor convergence, with the remainder increasing the mean water vapor of the atmosphere. Thus Kuo's method is here a very poor estimate of the total heating, and greatly overestimates the mean water vapor input to the convective layer.

Since $\overline{\omega^*} \sim \Sigma\omega^*$, one might approximately parameterise ω^* in terms of $\overline{\omega^*}$ and hence in terms of a low level convergence (not necessarily frictionally induced as in CISK models). However, the low level budgets cannot be expressed in terms of simply a mass transport ω^* on the cumulonimbus scale. Table 11 shows equivalent values $\hat{\omega}_r$, $\hat{\omega}_T$ defined to give the cumulonimbus modification without the lateral term, e.g.,

$$A_o \hat{\omega}_r \frac{\partial \overline{r}^2}{\partial p} = A_o \omega^* \frac{\partial \overline{r}^2}{\partial p} + \int_{\ell} C(r-\overline{r}^2)\ell d \qquad (6.1)$$

$\hat{\omega}_r$, $\hat{\omega}_T$ are comparable above 800 mb, but at the lowest levels have opposite sign (where cooling and drying is observed simultaneously). A detailed model of the surface (sub-cloud) layer is needed to accurately parameterise deep convection in terms of the large scale $\widetilde{\omega}$.

b) Factors influencing ω^*

Accurate parameterisation of ω^* , though necessary, is difficult, since the mean atmospheric changes $\Delta\overline{T}$, $\Delta\overline{r}$ (Tables 7, 8, 10) are small residuals whose sign depend primarily on the detailed vertical structure of $\widetilde{\omega}$ and ω^* , and hence on the complex structure of updraft and downdraft, growth and decay. The factors controlling $\omega^*(p)$ are still not clearly resolved, but some may be suggested.

i) The large-scale shear field may control the updraft-downdraft pattern and hence $\omega^*(p)$. It is hoped to study other classes of shear field than the one in this study in a future experiment.

ii) The transience of individual clouds is of importance. The cause may be the mid-level stabilisation observed during the

TABLE 11. EQUIVALENT MASS FLUXES TO GIVE CUMULONIMBUS MODIFICATION OF MEAN ATMOSPHERE (Eq. 6.1)

p mb	$\sum_L(-\omega^*)$ cgs	$\sum_L(-\hat{\omega}_T)$ cgs	$\sum_L(-\hat{\omega}_r)$ cgs	$(-\bar{\omega}^*)$ cgs
950	13	-90	46	(28)
900	37	-10	90	(38)
850	51	14	73	(31)
800	49	54	53	37
700	43	43	51	44
600	43	52	33	52
500	51	61	51	70
400	80	81	82	87
300	107	113	111	107
250	101	98		95
200	75	91		104
175	35	32		51
150	5	-24		4

Key (i) $\bar{\omega}^*$ values are from vapour budget below 800 mb.

(ii) $\hat{\omega}$ defined in 6.1.

e.g. $\sum_L (\hat{\omega}_r \frac{\Delta r}{\Delta p})_i = -(\frac{R_1 + R_2}{3R\ \Delta p})_i$ (R_1, R_2 defined in Table 9).

References

Betts, A. K., 1970, Unpublished Ph.D. Thesis, "Cumulus Convection". University of London.

Betts, A. K., 1972, "Non-Precipitating Cumulus Convection and Its Parameterisation". Submitted to Q.J.R.M.S. for publication.

Cruz, L., 1972, "Venezuelan Rainstorms as Seen by Radar". M.S. Thesis, Colorado State University.

Kuo, H. L., 1965, "On formation and intensification of tropical cyclones through latent heat release by cumulus convection". J. Atmos. Sci., 22, 40-63.

Morrissey, J. F. and Brousaides, F. J., 1970, "Temperature induced errors in the ML-476 humidity data". J. Appl. Meteor., 9, p. 805.

Ooyama, R., 1969, "Numerical simulation of the life-cycle of tropical cyclones". J. Atmos. Sci., 26, p. 3.

Pearce, R. P. and H. Riehl, 1968, "Parameterisation of convective heat and momentum transfer suggested by analysis of Caribbean data". Proc. WMO-IUGG Symp. Numerical Wea. Pred., Tokyo, I, p. 75.

Rasmussen, J. L., R. W. Furman and H. Riehl, 1969, "Moisture analysis of an extratropical cyclone". Arch. Meteor. Geoph. Biokl., Ser. A, 18, p. 275.

Riehl, H. and J. Malkus, 1958, "on the heat balance of the equatorial trough". Geophysica, Vol. 6, p. 503.

Appendix

The rawinsonde hygristor relative humidity (R.H.) was extrapolated to the surface, where a surface value was not recorded. Despite the presence of a superadiabatic layer this procedure gives the surface relative humidity to an accuracy of about 3% at Bowen ratios 0.8 and humidities 50% . This value was subtracted from an accurate surface value for R.H. obtained using a well ventilated aspirated psychrometer. A temperature difference (ΔT) between hygristor and thermistor was calculated from this R.H. difference, and used to correct the mixing ratio values at all pressure levels. No variation of ΔT with height was considered, although it should be realised that the thermal lag could vary with height (density and lapse-rate change), and further that scattered clouds can randomly affect the solar radiation error.

Theory:

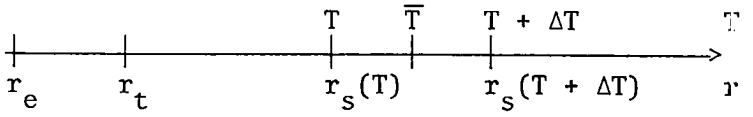

r_e denotes erroneous value

r_t denotes true value

$r_s(T)$ is saturation mixing ratio at (T)

T is thermistor temperature

$T + \Delta T$ is hygristor temperature

$\overline{T} = T + \Delta T/2$ a mean value

R = hygristor R.H.

Surface: Let

R_o = surface hygristor R.H.

$R_o + \Delta R_o$ = true surface R.H.

$$r_{to} = (R_o + \Delta R_o)\, r_s\,(T_o) = R_o\, r_s\,(T_o + \Delta T)$$

$$\therefore \frac{\Delta R_o}{R_o} = \frac{\Delta r_s}{r_s\,(T_o)}$$

$$\therefore \frac{\Delta R_o}{\overline{R}_o} = \frac{\Delta r_s}{\overline{r}_s}$$ where the bar denotes a mean value for the finite step $T_o \rightarrow T_o + \Delta T$.

$$= F\,(\overline{T})\,\Delta T \quad \text{where} \quad F\,(T) = \frac{L\,(T)}{R_V\,T^2}$$ (Clausius-Clapyron eq.)

R_V = gas constant for water vapor.

A value of ΔT can thus be computed from ΔR_o . This is taken as a constant for the sounding.

Above the surface:

R , T , ΔT are known

$$r_e = R\, r_s\,(T)$$

$$r_t = R\, r_s\,(T + \Delta T)$$

$$\Delta r = r_t - r_e = R\,\Delta r_s$$

Again from the Clausius-Clapyron eq.,

$$\Delta r_s = F\,(\overline{T})\, r_s\,(\overline{T})\,\Delta T$$

Other re-expressions are possible, e.g.,

$$r_s\,(\overline{T}) \quad r_s\,(T) + \Delta r_s/2$$

$$\therefore \Delta r_s = \frac{F\,(\overline{T})\, r_s\,(T)\,\Delta T}{1 - F\,(\overline{T})\,\Delta T/2}$$

$$\therefore \Delta r = r_e \frac{F\,(\overline{T})\,\Delta T}{1 - F\,(\overline{T})\,\Delta T/2}$$